Chemosensoric properties of porphyrin analogues ionized forms by spectrophotometry and quantum chemistry: 5,10,15,20-tetraphenyl-21-thia- and 5,10,15,20-tetraphenyl-21,23-dithiaporphyrins

Svetlana G. Pukhovskaya[a], Yulia B. Ivanova[b], Sergey A. Syrbu[b], Anna O. Plotnikova[a], Ilya A. Kuzmin[a], Oleg A. Pimenov[a] and Sergey A. Shlykov*[a].

[a] prof. Svetlana G. Pukhovskaya, Anna O. Plotnikova, Ilya A. Kuzmin, ass. prof. Oleg A. Pimenov, ass. prof. Sergey A. Shlykov
inorganic chemistry, physics and physical and colloidal chemistry
Ivanovo State University of Chemistry and Technology
Sheremetevskiy ave. 7, 153000 Ivanovo, Russian Federation
E-mail: shlykov@isuct.ru

[b] prof. Sergey A. Syrbu, ass. prof. Yulia B. Ivanova.
New materials based on macrocyclic compounds
G.A. Krestov Institute of Solution Chemistry of the Russian Academy of Sciences
Academicheskaya st.,1, 153045б , Ivanovo, Russia

Supporting information for this article is given via a link at the end of the document.

Abstract: Modification of porphyrins by a replacement of N atom(s) with a heteroatom(s), resulted in so called heteroporphyrins, exhibits interesting physicochemical properties. In this work, the spectral properties of ions and neutral forms of 5,10,15,20-tetraphenyl-21,23-dithia porphyrin (S_2PP) and 5,10,15,20-tetraphenyl-21-thia-porphyrin (HSPP) have been investigated. According to spectrophotometric analysis in acetonitrile – perchloric acid solution, the dication $H_2S_2PP^{2+}$ reveals an ability to coordinate two ClO_4^- anions, which not happens for H_3SPP^{2+}. This fact observed in UV–Vis absorption spectra indicates the possibility of exhibiting chemosensory properties of S_2PP molecules. Geometries of the neutral and ionized forms were derived from B3LYP/cc-pVTZ calculations. Perimeters of the cavities increase in the series: H_2PP–HSPP–S_2PP. This trend is kept for the ionized forms; protonation expands the cavity perimeter. Electron density distributions were analyzed in terms of quantum theory atoms in molecule (QTAIM). The UV-vis spectra simulated by TDDFT fits with the experimental results.

Introduction

The porphyrins are a class of natural pigments and aromatic macrocycles ‘constructed' from four pyrroles that are fully conjugated with four meso-carbons. They play an important role in living organisms. Also, due to ease of modification, the porphyrins have myriad of applications, including biomedicine [1–7], catalysis [8–11] and materials [12–17].

One of the promising directions for the development of modern science is the creation of new effective molecular sensors, allowing determination of concentrations of various ions in solutions with high sensitivity and selectivity as dominating demands.

Various approaches are applied to modify compounds of this class. Firstly, it is a functionalization of porphyrins by introduction of peripheral substituents. Second is a core-modification of porphyrins by replacement of one or two pyrrole N atoms by heteroatoms such as C, O, S, Se, Te, P, Si, etc. resulted in so called heteroporphyrins. The latter exhibit interesting physicochemical properties different from the regular porphyrins [18–20]. Specifically, the heteroporphyrins have an ability to stabilize metals in unusual oxidation states, such as Cu(I) and Ni(I) [21–29]. However, most of the published results on heteroporphyrins are limited by the preparation of different metal derivatives and the exploration of their structural, spectroscopic and electrochemical properties [21,22,30–35].

In our recent work, the absorption and luminescence spectroscopy was applied for 21-thia- and 21,23-dithia-5,10,15,20-tetraphenylporphyrins solutions in acetonitrile [36]. The Spin-orbit couplings in the macrocycle were applied to interpret the fluorescence quantum yields and fluorescence quenching of the heteroporphyrins.

Of a specific interest, a mechanism of the counter ion coordination which involves a protonation of the porphyrin ring [37]. The ionized tetrapyrrole compounds have a great potential in nonlinear optics [38]. The protonation of free-base porphyrins and their structural analogues is one of the fundamental and most important reactions. Several studies have reported the protonation and deprotonation of porphyrinoids [39–41].

Due to the both, steric and electronic repulsions, the two hydrogen atoms in the central cavity of the free-base porphyrins occupy the opposite positions in the neutral state. However, a move of these atoms to the adjacent imino nitrogens is possible. The latter easily undergo protonation in acidic media. N_4-porphyrins exhibit similar equilibrium constants for the first (K_1) and second protonation (K_2); therefore detecting the monoprotonated species by the ^{1}H NMR and UV-vis spectroscopies [42,43].

It should be noted that the acid-base properties of porphyrinoids and especially heteroporphyrins are not extensively investigated. In contrast to the protonation behavior of N_4-porphyrins, that of the thiaporphyrins (S-core-modified porphyrins) has been seldom studied, although the stepwise protonation for N_3S-porphyrins is believed to occur [44,45].

In the present study, the UV-visible absorption spectroscopy data for S-core-modified heteroporphyrins 5,10,15,2-tetraphenyl-21-thiaporphyrin (**I** or HSPP) and

5,10,15,20-tetraphenyl-21,23-dithiaporphyrin (**II** or S_2PP) represented partially in our recent work [46] are supported by acid-base properties of **I** and **II** obtained by spectrophotometric titration with perchloric acid solutions in acetonitrile and compared with the previously studied 5,10,15,20-tetraphenylporphyrin (**III** or H_2PP). For explanation of experimental part, spectroscopic data and acid-base properties, the time-dependent density functional theory (TDDFT) calculations were involved to simulate UV-visible spectra. In addition, the quantum theory of atoms in molecules (QTAIM) was applied to explore the coordination properties of **I** and **II**.

Results and Discussion

Spectrophotometric analysis

Porphyrine H_2PP **III** in organic solvents exhibit amphoteric properties and, in the presence of acids and bases, can be protonated and deprotonated at intracycle nitrogen atoms. In a first approximation (without participation of a solvent and stabilization of the formed particles by counterions), the processes of acid-base interaction of porphyrins can be described by the equations (1-4) [47]:

$$H_3PP^+ \overset{K_{b1}}{\rightleftarrows} H_2PP + H^+, \quad (1)$$

$$H_4PP^{2} \overset{K_{b2}}{\rightleftarrows} {}^{+}H_3PP^+ + H^+, \quad (2)$$

$$H_2PP \overset{K_{a1}}{\rightleftarrows} HPP^- + H^+, \quad (3)$$

$$HPP^- \overset{K_{a2}}{\rightleftarrows} PP^{2-} + H^+, \quad (4)$$

where H_2PP, HPP^-, PP^{2-}, H_3PP^+, H_4PP^{2+} are neutral, cation and dication forms of the porphyrin ligand; K_{ai} and K_{bi} are acidity and basicity constants, respectively.

In this work, the acid-base properties of ligands **I** and **II** were studied by spectrophotometric titration in binary solutions CH_3CN-$HClO_4$ and CH_3CN-$(C_2H_5)_4NClO_4$ at 298 K in a wide range of titrant concentrations. During the experiment, mono- and dicationic forms of ligands were fixed and isolated. This made it possible to obtain supramolecular systems for compound **II** with ClO^{4-} anions present in the solution. However, the doubly protonated form of ligand **I** did not show such properties. In CH_3CN-$HClO_4$ solutions, reactivity analysis showed that compound **II** has very weak basic properties compared to **I** and **III**; for which it was partially studied earlier (see, for example, [47]).

However, for all (**I**, **II** and **III**) compounds, the dissociation processes of the protonated forms represented by equations (1) and (2) were observed experimentally, which makes it possible to study and compare their basicity properties. It is known that upon protonation the symmetry of the molecules changes [48]. Suggested shapes of cation and dication forms of **I**-**III** are illustrated in ESI (Schemes S1-S3). The main conjugation contours of the molecules and ions H_2PP, H_3PP^+ and H_4PP^{2+} are aromatic formed by 18 π-electrons. But, as follows from Schemes S1-S3, the sizes, charges and symmetries are different [49,50]. For this reason, all acid-base forms of porphyrins are intensely colored but have characteristic differences in electronic absorption spectra.

The UV-Vis spectra of **I** and **II** in CH_3CN upon titration with 0.01M $HClO_4$ solutions are plotted in Figure 1 and 2. Under these conditions, perchloric acid is in a completely dissociated form, and protonation occurs due to the solvated proton [51].

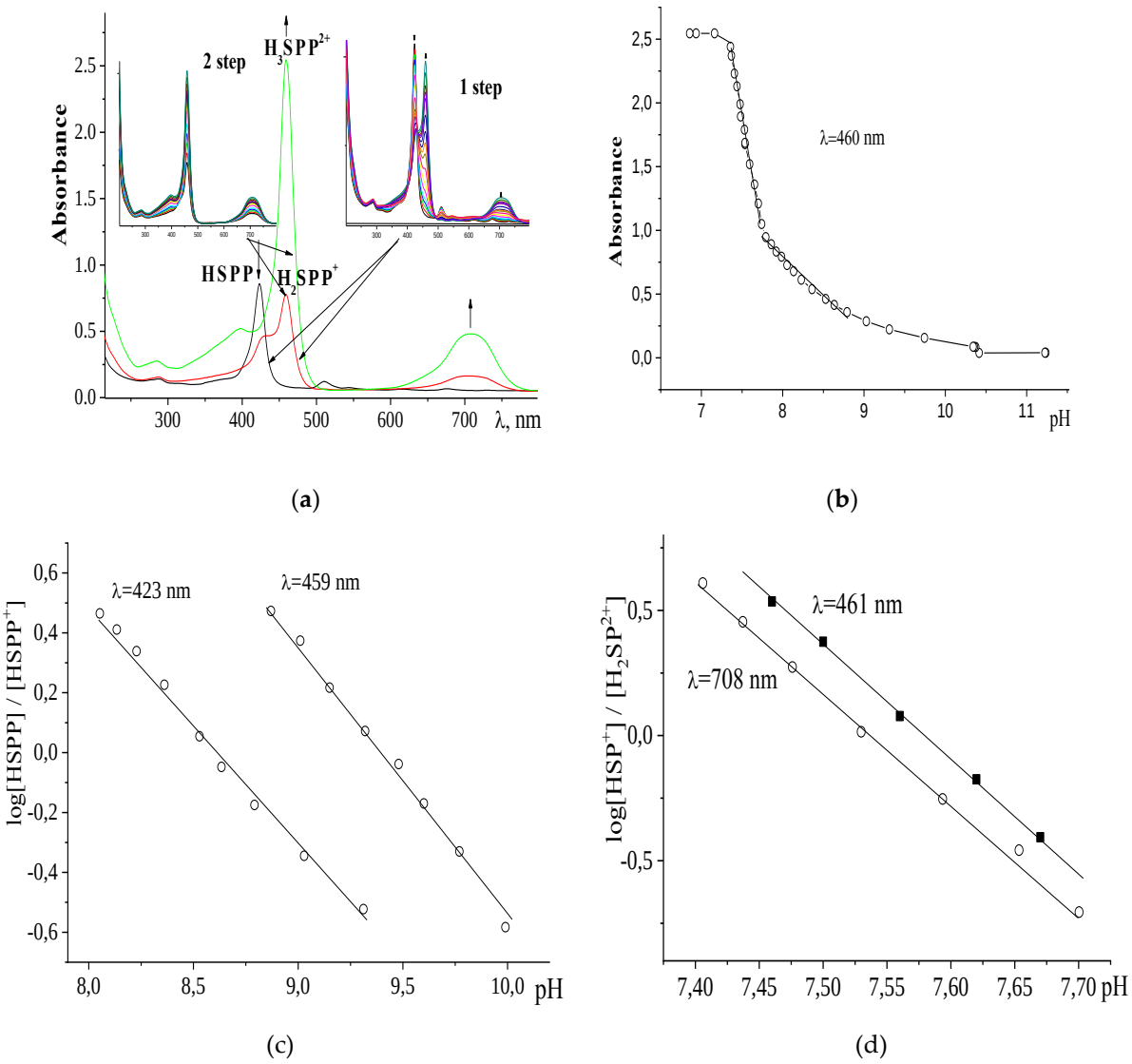

Figure 1. (a) Changes in the UV/Vis spectra of ligand I, C_{porph}=2.33·10^{-6} mol/L, in the CH_3CN-$HClO_4$ (0-3.01·10^{-4} mol/L) system, hereinafter, concentrations of $HClO_4$ are given in brackets; **1st stage** (0-1.40·10^{-4} mol/L); **2nd stage** (1.40·10^{-4} - 3.01·10^{-4} mol/L);
(b) optical density A of ligand **I** vs. pH for the range specified in (a), λ=460 nm;
(c) and (d) plots of log*Ind* vs. pH for the **1st** and **2nd stages** of ligand **I** protonation. *Ind* is an indicator ratio: *Ind*=[HSPP]/[H_2SPP^+] and [H_2SPP^+]/[H_3SPP^{2+}] for the stages **1** and **2**, respectively.

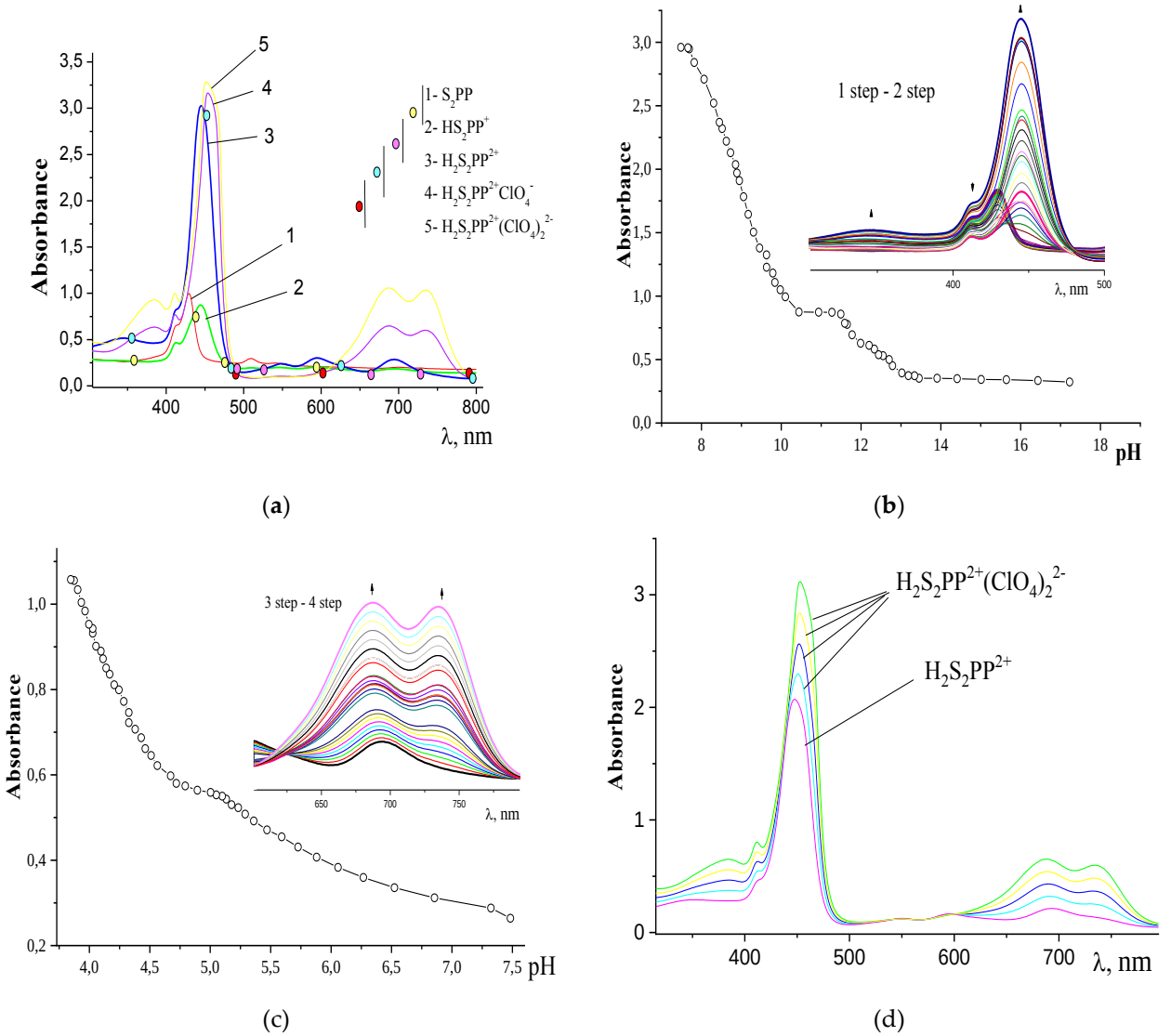

Figure 2. (a) Changes in the UV-Vis spectra of ligand **II**, Cporph=4.98·10^{-6} mol/L, in the CH_3CN-$HClO_4$ (0-4.08·10^{-3} mol/L) system; **1st** to **4th stages**; hereinafter, concentrations of $HClO_4$ are given in brackets;
(b) 1st and 2nd stages (0-1.77·10^{-4} mol/L), optical density A of ligand **II** vs. pH, λ=429 nm;
(c) 3rd and 4th stages (1.77·10^{-4} - 4.08·10^{-3} mol/L), optical density A of ligand **II** vs. pH, λ=686 nm;
(d) Changes in the UV-Vis spectra upon titration of dication of **II** ($H_2S_2PP^{2+}$) by solution $(C_2H_5)_4NClO_4$ (0.01 mol/L); in ACN, a $H_2S_2PP^{2+}(ClO_4^-)_2$) form is obtained, 298 K.

Analysis of the UV-Vis spectra showed that as the concentration of $HClO_4$ in the **I**-$HClO_4$-CH_3CN system increases, the formation of two groups of isosbestic points was observed, which is due to the presence of two individual equilibria between the pairs of light-absorbing centers, $HSPP/H_2SPP^+$ and H_2SPP^+/H_3SPP^{2+}, see Figure S1 [47]. The spectrophotometric titration curve, Figure 1(b), and the dependence of log*Ind* vs pH, Figure 1(c, d) and the footnote for definition of *Ind*, based on the experimental data for each ligand protonation stage at different wavelengths confirmed a stepwise interaction of porphyrin **I** with $HClO_4$.

Considering the basic dissociation processes of the protonated forms, Equation (1) and (2), material-balance equation (5) and the current concentration of all forms (6), subject to the Lambert-Bouger-Beer law, the following concentration distributions of the molecular and protonated forms for **I** in the CH_3CN – $HClO_4$ system (Figure S1) were expressed (equations 7, 8, 9):

$$C_o=100\%=[HSPP]+[H_2SPP^+]+[H_3SPP^{2+}], \quad (5)$$

$$A_t=(A_{HSPP}\cdot K_{b1}\cdot K_{b2}+ A_{H2SPP}{}^{+}\cdot a\cdot K_{b1}+a^2\cdot A_{H3SPP}{}^{2+})/ /(K_{b1}\cdot K_{b2}+a\cdot K_{b2}+a^2), \quad (6)$$

$$[HSPP]=K_{b1}\cdot K_{b2}/(K_{b1}\cdot K_{b2}+a\cdot K_{b2}+a^2)\cdot 100\%, \quad (7)$$

$$[H_2SPP^+]=a\cdot K_{b2}/(K_{b1}\cdot K_{b2}+a\cdot K_{b2}+a^2)\cdot 100\%, \quad (8)$$

$$[H_3SPP^{2+}]=a^2/(K_{b1}\cdot K_{b2}+a\cdot K_{b2}+a^2)\cdot 100\%, \quad (9)$$

where [HSPP], $[H_2SPP^+]$, $[H_3SPP^{2+}]$ are concentrations of the corresponding forms in %; $a=10^{(-pH)}$ – hydrogen ion activity; K_{b1} and K_{b2} – basicity constants of the processes (1) and (2), respectively; A_t , A_{HSPP} , A_{H2SPP+} and $A_{H3SPP2+}$ are total (t) and individual optical densities of the molecular and ionized forms.

For the compound **II**, during the titration in the CH_3CN-$HClO_4$ system, four families of spectral curves were revealed, each corresponded to its own set of isosbestic points (Figure 2a), indicating the sequential course of four processes. It was shown in [52,53] that the dication of the porphyrin H_4PP^{2+} macrocycle can in some cases exhibit the properties of an anion-molecular receptor. The intracyclic NH groups are able to coordinate the base molecules of various nature (solvent molecules Sol. and anions An^-) with formation of individual and/or mixed complexes $[[H_4PP^{2+}](Sol.)_2$, $[H_4PP^{2+}](An^-)(Sol.)$, $(H_4PP^{2+})(An^-)_2$. It is known that CH_3CN is a solvent weakly solvating both cationic and anionic species [48,54]. At the same time, the protonation depth (the depth of proton incorporation into the electron shell of the donor atom) in this solvent is quite high, since the protons in the solution are initially weakly bound by the solvent and the degree of specific solvation at the central atoms is small.

It is likely that in the case of the **II**-CH_3CN-$HClO_4$ system, the processes of sequential addition of two protons, **1st- 2nd** titration stages (see Equations. (1,2) and Figure 2 (a,b)) occur, and possibly, followed by the addition of the first and the second ClO_4^- ions, **3rd** and **4th** titration stages (Figure 2 (a,c), Equations. (10,11)), respectively.

$$(H_2\ S_2PP^{2+})ClO_4^- \overset{K_{x1}}{\rightleftarrows} (H_2S_2PP^{2+})+ClO_4^-\cdot K_{x1} \quad (10)$$

$$H_2S_2PP^{2+})(ClO_4^-)_2 \overset{K_{x2}}{\rightleftarrows} (H_2S_2PP^{2+})ClO_4^- + ClO_4^-\ K_{x2} \quad (11)$$

$$C_o=100\%=C(S_2PP)+C(HS_2PP^+)+C(H_2S_2PP^{2+})+ +C(H_2S_2PP^{2+}ClO_4^-)+C(H_2S_2PP^{2+}(ClO_4^-)_2) \quad (12)$$

$$A_t = (A_{PS2}\cdot K_{b1}\cdot K_{b2}\cdot\ K_{x1}\cdot K_{x2} + A_{HPS2}{}^{+}\cdot K_{b2}\cdot K_{x1}\cdot K_{x2}\cdot a+ +A_{H2S2PP}{}^{2+}\cdot a^2\cdot K_{x1}\cdot K_{x2}+A_{H2S2PP}{}^{2+}{}_{ClO4}{}^{-}\cdot\ a^2\cdot\ K_{x2}\cdot[ClO_4^-] + +A_{H2S2PP}{}^{2+}{}_{(ClO4}{}^{-}{}_{)2}\cdot a^2\cdot[ClO_4^-]^2)/(K_{b1}\cdot K_{b2}\cdot K_{x1}\cdot K_{x2}+ +a\cdot K_{b2}\cdot K_{x1}\cdot K_{x2}+a^2\cdot K_{x1}\cdot K_{x2}+a^2\cdot K_{x2}\cdot[ClO_4^-]+ a^2\cdot[ClO_4^-]^2) \quad (13)$$

On the basis of Equations. (1, 2, 12, 13) and the Beer-Lambert-Bouguer law, one can derive the concentration distributions of all the spectrally distinct forms for the studied compound **II** (14-18) in the CH_3CN-$HClO_4$ system, Figure S2.

$$[S_2PP]=100\%\cdot K_{b1}\cdot K_{b2}\cdot K_{x1}\cdot K_{x2}/(K_{b1}\cdot K_{b2}\cdot K_{x1}\cdot K_{x2}+a\cdot K_{b2}\cdot \cdot K_{x1}\cdot K_{x2}+a^2\cdot K_{x1}\cdot K_{x2}+a^2\cdot K_{x2}\ [ClO_4^-]+ +a^2\cdot[ClO_4^-]^2) \quad (14)$$

$$[HS_2PP^+]=100\%\cdot a\cdot K_{b2}\cdot K_{x1}\cdot K_{x2}/(K_{b1}\cdot K_{b2}\cdot K_{x1}\cdot K_{x2}+a\cdot K_{b2}\cdot K_{x1}\cdot \cdot K_{x2}+a^2\cdot K_{x1x2}+a^2\cdot K_{x2}\cdot[ClO_4^-]+a^2\cdot[ClO_4^-]^2) \quad (15)$$

$$[H_2S_2PP^{2+}]=100\%\cdot a^2\cdot K_{x2}\cdot K_{x1}/(K_{b1}\cdot K_{b2}\cdot K_{x1}\cdot K_{x2}+a\cdot K_{b2}\cdot K_{x1}\cdot \cdot K_{x2}+a^2\cdot K_{x1}K_{x2+}+a^2\cdot K_{x2}\cdot[ClO_4^-]+a^2\cdot[ClO_4^-]^2) \quad (16)$$

$$[H_2S_2PP^{2+}(ClO_4^-)]=100\%\cdot a^2\cdot K_{x2}[ClO_4^-]/\ (K_{b1}\cdot K_{b2}\cdot K_{x1}\cdot K_{x2}+ +a\cdot K_{b2}\cdot K_{x1}\cdot K_{x2}+a^2\cdot K_{x1}\cdot K_{x2}+a^2\cdot K_{x2}\cdot[ClO_4^-]+a^2\cdot[ClO_4^-]^2) \quad (17)$$

$$[H_2S_2PP^{2+}(ClO_4^-)_2]=100\%\cdot\ a^2\cdot[ClO_4^-]^2/(K_{b1}\cdot K_{b2}\cdot K_{x1}\cdot K_{x2}+ +a\cdot K_{b2}\cdot K_{x1}\cdot K_{x2}+a^2\cdot K_{x1}\cdot K_{x2}+a^2\cdot K_{x2}\cdot\ [ClO_4^-]+ a^2\cdot[ClO_4^-]^2), \quad (18)$$

All figures and tables where $[S_2PP]$; $[HS_2PP^+]$; $[H_2S_2PP^{2+}]$, $[H_2S_2PP^{2+}(ClO_4^-)]$, $[H_2S_2PP^{2+}(ClO_4^-)_2]$ are concentrations of the corresponding forms in (%); $a=10^{(-pH)}$ – hydrogen ion activity; K_{x1} and K_{x2} – basicity constants of the processes (10) and (11), respectively; A_t, A_{S2PP}, $A_{HS2PP}{}^{2+}$ and $A_{H2S2PP}{}^{2+}$ $A_{H2S2PP}{}^{2+}{}_{(ClO4}{}^{-})$, $A_{H2S2PP}{}^{2+}{}_{(ClO4}{}^{-}{}_{)2}$ are total (t) and individual optical densities of the molecular and ionized forms.

Bearing in mind the weak coordinating ability of CH_3CN, it is obvious that the interaction of the ligand with the solvent gives no significant influence, and the processes (10, 11) can be separated. To confirm our assumption, the following experiment was performed: the region of the concentration $HClO_4$ where the dication form $H_2S_2PP^{2+}$ exists was calculated by equation (16) resulted in pH ~ 7.5 (see the maximum in Figure S2), then the reaction mixture was brought to that pH value with the followed titration by CH_3CN solution $(C_2H_5)_4NClO_4$ – (0.01 mol/l). Upon this titration, the UV-Vis spectra changed manifesting a bathochromic shift, Figure 2d, which is to be assigned to a transition from the dication $H_2S_2PP^{2+}$ to the associated form $H_2S_2PP^{2+}(ClO_4^-)_2$. It is to be pointed out, that the possibility of the associative processes between a dication and perchlorate ions relevant to **II** was not observed in the analogous experiment with **I**.

The quantitative values of the stepwise and the total constants of the basic ionization for the studied compounds at 298 K were calculated according to equation (19). Their corresponding values and the parameters of the UV-Vis spectra of the molecular and ionized forms in the CH_3CN - $HClO_4$ system are listed in Table 1.

$$pK=-\log K=pH-\log Ind \quad (19)$$

Where *K* is the constant for the 1st, 2nd (K_{b1} and K_{b2}), 3rd and 4th (K_{x1} and K_{x2}), titration stages , *Ind* – the indicator ratio: $Ind=[HSPP]/[HSPP^+]$ and $[HSPP^+]/[H_2SPP^{2+}]$ for **I** and $[S_2PP]/[HS_2PP^+]$, $[HS_2PP^+]/[H_2S_2PP^{2+}]$, $[H_2S_2PP^{2+}]/[H_2S_2PP^{2+}ClO_4^-]$, $[H_2S_2PP^{2+}ClO_4^-]/[H_2S_2PP^{2+}(ClO_4)_2{}^{2-}]$ for **II**, respectively; $pH=-2.48-2.65\cdot\log C_{HClO4}$ [43]; an uncertainty of the constants measurement did not exceed 3-5%.

Table 1. Basic ionization constants logarithms pK_{b1}, pK_{b2} pK_{x1}, pK_{x2} and spectral characteristics of molecular and protonated forms of porphyrins **I-III** in CH_3CN-$HClO_4$ system at 298K

	Porphyrin	λ (logε)[a]					pK_{b1}	pK_{b2}	$\sum pK_b$ [b]
I	HSPP	423(5.56)	510(4.49)	544_{sh}(3.90)	616(3.63)	676(3.83)	8.76	7.48	16.24 [4ду7]
	H_2SPP^+	430(5.29)	459(5.60)	-	-	708(4.20)			
	H_3SPP^{2+}	395_{sh} (5.34)	460(5.11)	-	-	710(5.39)			
II	S_2PP	412_{sh}(5.12)	429(5.30)	509(4.36)	541(3.80)	700(3.66)	12.25	8.95	21.20
	HS_2PP^+	413_{sh}(4.97)	444(5.24)	546(4.19)	594(3.70)	693(3.66)			
	$H_2\ S_2PP^{2+}$	345(5.01)	445 (5.37)	548(3.77)	594(3.83)	694(3.82)			
	$H_2\ S_2PP^{2+}ClO_4^-$	381_{sh}(5.10)	412 (4.77)	451(5.39)	689(4.17)	738(4.12)	pK_{x1}	pK_{x2}	$\sum pK_x$ [c]
	$H_2S_2PP^{2+}(ClO_4^-)_2$	385_{sh}(5.27)	411(5.30)	454(5.82)	686(5.33)	735(5.32)	5.93	4.29	10.22
III	H_2PP	413(5.02)	512(3.56)	546(3.12)	589(2.92)	646(2.96)	-	-	18.67[43]
	H_4PP^{2+}	441(5.04)	-	-	-	661(4.17)			19.8 [47]

[a] uncertainty for the extinction coefficients ε based on three sets of measurements was derived as 1-3%; λ in nm;
[b] $\sum K = K_{b1} \cdot K_{b2}$
[c] $\sum K = K_{x1} \cdot K_{x2}$

The basicity decrease of 21-thia-substituted porphyrin (**I**) as compared to that of H_2PP (Table 1) is obviously due to the presence of a less electronegative sulfur atom in the macrocycle reaction center – the relative Pauling ENs are 2.5 (S) and 3.0 (N) [55]. Moreover, the total basicity index increases when change from **I** to **II**, apparently, manifested in the ClO_4^- anions protonation and association of processes superposition. Probably, the pK_{b1}, pK_{b2}, pK_{x1} and pK_{x2} values for **II** are composite quantities that include associative interaction with the anion. The resultant p*K* values, due to the formation of complexes of $H_2S_2PP^{2+}$ with ClO_4^-, are the sum of the stepwise values $\log K_{b1}$ and $\log Kx_1$ of the $[H_2S_2PP^+ClO_4^-]$ formation, and analogously, of the $\log K_{b2}$ and $\log Kx_2$ of the $[H_2S_2PP^{2+}(ClO_4^-)_2]$ formation, due to ionic bonds, which are characterized by lower values of the stability constants.

Structure, chemical bonding and simulation of electronic spectra by quantum chemical calculations.

The QC modeling of tetraphenylporphyrin with one (**I**) and two (**II**) sulfur heteroatoms introduced into the central cavity was aimed at exploring the relations between peculiarities of geometric and electronic structures with the experimental electronic absorption spectra. Additional attention was paid to coordinating ability changes caused by the mentioned N-to-S substitution as well as by protonation and its facilitation to the perchlorate anion coordination.

Hereinafter, we will discuss the results with PCM (acetonitrile) applied, unless otherwise stated.

Geometries of neutral and ionized species.

The B3LYP/cc-pVTZ calculations for the **neutral** forms of the mono- (**I**) and dithio (**II**) substituted porphyrins resulted in practically planar structures of cavities with the phenyl groups are turned by ca. 25° with respect to the plane. This does not produce essential difference with the parent, H_2PP (**III**), compound, see, for example [56] and our results in ESI.

Exploring the adjacent and opposite locations of the S atom in **II** showed a significant preference of the latter, by 8.5 kcal/mol, apparently due to steric reasons, see also [57,58].

The summarized lengths of the bonds forming the central cavity (see Figure S3) increase upon substitution in the series: 22.17 (**III**), 22.94 (**I**) and 23.70 (**II**) Å. This trend appeared to be also kept for the cation and dication forms. The protonation leads to expansion of the cavities' perimeter: 22.98 (**I**) 23.73, (**II**) Å (cations) and 23.05 (**I**), 23.79 (**II**) Å (dications). Noticeably, that in the dications, the location of the H atoms in the cavities are sterically hindered, that leads to significant misstatement of the ligand's planar structure. The molecular models and atom numbering of **I** and **II** are given in Figure 3.

The solvation has an effect on geometry, atomic charges and electronic absorption spectra. Introduction of the ACN solvent in terms of the PCM model resulted in changes not exceeding 0.004 Å for distances and 0.3° for angles, that for all neutral and ionized species seems negligible.

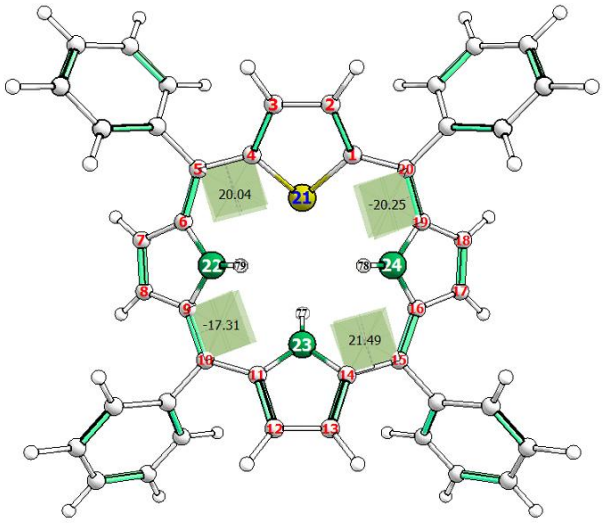

H_3SPP^{2+}-C_s

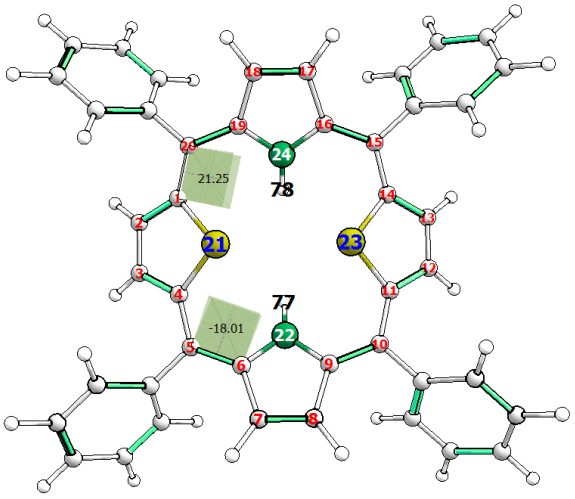

$H_2S_2PP^{2+}$ C_{2v}

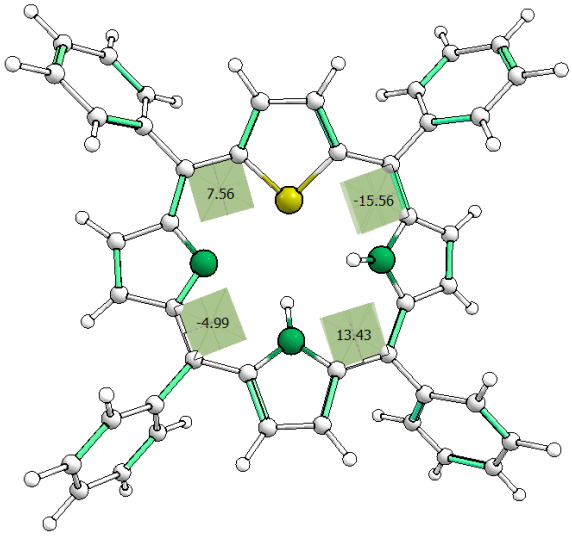

H_2SPP^{+} C_1

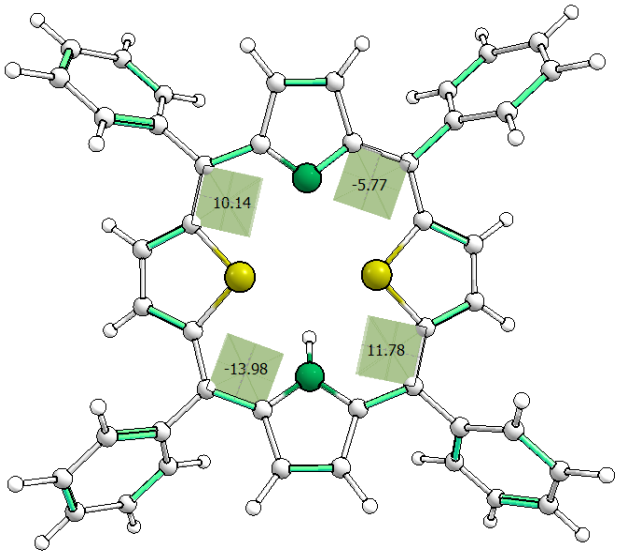

HS_2PP^{+} C_s

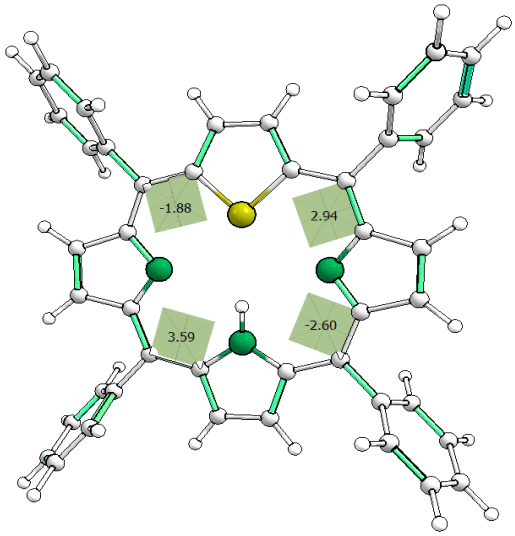

HSPP Cs

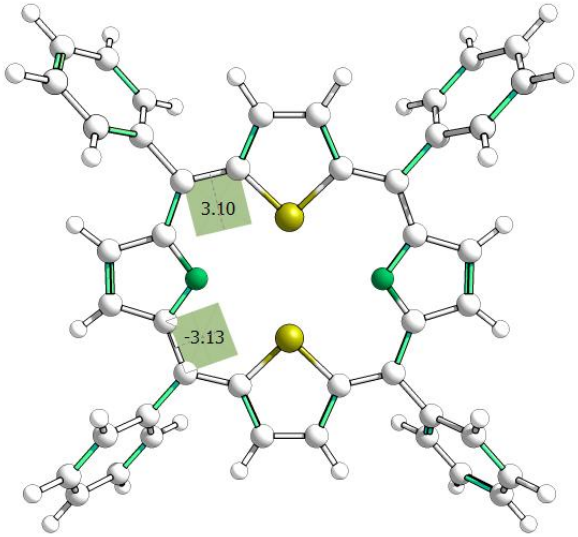

S_2PP C_{2v}

Figure 3. Structure of neutral and ionized porphyrins **I** and **II** calculated at B3LYP/cc-pVTZ level with atom numbering. The indicated parameters are the dihedral angles between the bonds inside the central cavity relative to the C_{meso}–C_{alpha} bonds.

QTAIM results, charges of atoms.

Influence of a solvent. Unlike a weak influence on the geometry, the environment causes, nevertheless, a more pronounced change on the charges, especially in dication protonated forms: the $S_{21,23}$ and $H_{78,77}$ atoms in the central ring of $H_2S_2PP^{2+}$ get more positive charge: +0.243*e* and +0.457*e* (ACN) *vs* +0.199*e* and +0.436*e* (gas), respectively; for other atoms the differences are within 0.015*e*.

Similar tendency is observed in case of H_3SPP^{2+} for S_{23} and $H_{25,78,77}$ atoms. However, the C atoms which have a link with the N or S atoms also become more positive: the charges on $C_{1,4}$ are +0.353*e* (gas) and +0.383*e* (ACN), but for $C_{11,14}$ are -0.172 *e* (gas) and -0.163*e* (ACN). For the singly protonated forms HS_2PP^+ and H_2SPP^+ these differences are limited by 0.01*e*.

Influence of protonation. In the *gas phase*, the H^+ ion addition into the porphyrin core changes the charges as: –1.098e to –1.190e (N) and +0.377e to +0.199e (S) for the $S_2PP \rightarrow H_2S_2PP^{+2}$ transition and –1.108e to –1.185e (N) and +0.345e to +0.172e (S) for the $HSPP \rightarrow H_3SPP^{+3}$ transition. In *acetonitrile*, the same tendencies are observed but in a less pronounced way, mainly for the N and S atoms: –1.113e to –1.187e (N): +0.333e to +0.243e (S) for the $S_2PP \rightarrow H_2S_2PP^{+2}$ transition and –1.121e → –1.182e (N) and +0.303e → +0.230e (S) for the $HSPP \rightarrow H_3SPP^{+3}$ transition.

The bond critical points (BCP) between $S_{21}…S_{23}$ and $S_{21}…H_{77}$ (in **S_2P** and **HSP**, respectively) possess a low electron density (ρ), relatively small positive value of Laplacian ($\nabla^2\rho_b$) and a negative, but close to zero, value of local electronic energy density (H_b), see Tables 2 and 3. All these characteristics correspond to intermediate, in terms of the QTAIM terminology, interactions that describe the $S_{21}…S_{23}$, $S_{21}…N_{22}$ or $S_{21}…H_{77}$ chemical bonding in the central hetero-porphyrin ring (cavity). The Laplacian map (Figure S4) shows the regions of a local charge depletion ($\nabla^2\rho_b > 0$) and concentration ($\nabla^2\rho_b < 0$).

Upon double protonation $S_2PP \rightarrow H_2S_2PP^{+2}$, the electron density in the BCPs decreases almost twice for the $S_{21}…S_{23}$ bond, whereas only by 20% for the $S_{21,23}…N_{22,24}$ bond, see Table 2. This also leads to the $S_{21}…S_{23}$ and $S_{21,23}…N_{22,24}$ distances increase: 3.067→ 3.447 and 2.780 → 3.003 Å, respectively that may be attributed to the influence of the $H_{77,78}$ atoms. The positively charged hydrogens $H_{77,78}$ (+0.457*e*) in $H_2S_2PP^{2+}$, push the positive sulfurs $S_{21,23}$ and pulls the negative nitrogens $N_{22,24}$ away from the core plane, thereby stretching the central core.

The delocalization indices δ(A|B), Table 2, designate that the S-C and N-C bond orders in $H_2S_2PP^{2+}$ are almost the same and correspond to a single bonding; same is relevant to H_3SPP^{2+} (Table S1 in ESI). Based on that, one may suggest a similarity of the conjugated systems in $H_2S_2PP^{2+}$ and H_3SPP^{2+}.

Table 2. The BCPs and their parameters [a] for the neutral and protonated forms of **II**

Porphyrine	Interaction	R_e	$\Delta\rho$	$\nabla^2\rho$	ε	H_b	δ(A|B)
S_2PP	***r*($S_{21}…S_{23}$)**	**3.067**	0.018	+0.058	0.226	-0.001	0.125
	***r*($S_{21,23}…N_{22,24}$)**	**2.780**	0.020	+0.068	0.077	-0.002	0.134
	***r*($S_{21,23}$–$C_{1,4,11,14}$)**	**1.750**	0.207	-0.381	0.219	+0.160	1.187
	***r*($N_{22,24}$–$C_{6,9,16,19}$)**	**1.353**	0.341	-1.040	0.142	+0.467	1.230
HS_2PP^{1+}	***r*($S_{21}…S_{23}$)**	**3.201**	0.015	0.047	0.194	-0.001	0.105
	***r*($S_{21,23}…H_{77}$)**	**2.392**	0.019	0.064	0.030	-0.002	0.127
	***r*(N_{24}–H_{77})**	**1.008**	0.350	-2.079	0.031	0.572	0.694
	***r*($S_{21,23}…N_{22}$)**	**2.813**	0.019	0.064	0.030	-0.002	0.127
	***r*($S_{21,23}$–$C_{4,11}$)**	**1.754**	0.205	-0.370	0.210	0.156	1.183
	***r*($S_{21,23}$–$C_{1,14}$)**	**1.739**	0.211	-0.395	0.220	0.164	1.194
	***r*(N_{22}–$C_{6,9}$)**	**1.353**	0.341	-1.043	0.137	0.467	1.231
	***r*(N_{24}–$C_{16,19}$)**	**1.373**	0.314	-0.854	0.143	0.446	1.067
$H_2S_2PP^{+2}$	***r*($S_{21}…S_{23}$)**	**3.447**	0.010	0.032	0.089	-0.001	0.075
	***r*($S_{21,23}…N_{22,24}$)**	**3.003**	0.015	0.053	0.488	-0.002	0.068
	***r*($N_{22,24}$–$H_{77,78}$)**	**1.007**	0.351	-2.095	0.031	0.575	0.709
	***r*($S_{21,23}$–$C_{1,4,11,14}$)**	**1.749**	0.206	-0.371	0.214	0.157	1.190
	***r*($N_{22,24}$–$C_{6,9,16,19}$)**	**1.372**	0.315	-0.857	0.141	0.448	1.069

[a] R_e - the equilibrium distance (Å); $\Delta\rho$ – electron density (e/Bohr^3); $\nabla^2\rho$ - the Laplacian of the electron density (e/Bohr^5); ε - the bond ellipticity; H_b– local electronic energy density (Hartree/Bohr^3), δ(A|B) – the electron delocalization index, e;

Table 3. The BCPs and their parameters [a] for the neutral and protonated forms of **I**

Porphyrin	**Interaction**	**R_e(Å)**	ρ	$\nabla^2\rho$	ε	H_b	**δ(A|B)**[b]
HSPP	***r*($N_{22,24…}H_{77}$)**	**2.448**	0.011	+0.043	0.339	-0.002	0.024
	***r*($S_{21}…H_{77}$)**	**2.547**	0.011	+0.038	0.262	-0.001	0.033
	***r*(N_{23}–H_{77})**	**1.011**	0.346	-2.126	0.034	+0.579	0.675
	***r*($S_{21}…N_{22,24}$)**	**2.698**	0.025	+0.079	0.110	-0.001	0.174
H_2SPP^+	***r*($S_{21}…H_{77}$)**	**2.680**	0.009	0.031	0.367	-0.001	0.027
	***r*($S_{21}…N_{22}$)**	**2.827**	0.022	0.075	0.756	-0.002	0.104
	***r*(N_{22}–H_{78})**	**1.008**	0.351	-2.056	0.034	0.567	0.718
	***r*($N_{23}…N_{22}$)**	**3.110**	0.008	0.034	0.158	-0.002	0.026
	***r*(N_{23}–H_{77})**	**1.009**	0.348	-2.083	0.033	0.570	0.703
	***r*($S_{21}…N_{24}$)**	**2.729**	0.023	0.074	0.063	-0.001	0.163
	***r*($N_{24}…H_{77}$)**	**2.396**	0.012	0.047	0.249	-0.002	0.029
H_3SPP^{2+}	***r*($S_{21}…H_{25}$)**	**3.102**	0.004	0.015	0.141	-0.001	0.011
	***r*($N_{22,24}$–$H_{78,79}$)**	**1.007**	0.351	-2.075	0.033	0.570	0.724
	***r*(N_{23}–H_{77})**	**1.009**	0.349	-2.025	0.035	0.557	0.738
	***r*($S_{21}…N_{22,242}$)**	**2.933**	0.016	0.059	0.734	-0.002	0.085
	***r*($N_{23}…N_{22,24}$)**	**3.088**	0.008	0.036	2.119	-0.002	0.030

[a] – See footnotes for Table 2; [b] – see also Table S1 in ESI for the δ(A|B) indices for the S-C and N-C bonds are given.

An important parameter is a summarized charge of the central cavity which is an identifier of a possibility of the molecule to coordinate other ions, molecules or atoms. The central cavity involves the N, S and H atoms: $S_{21,23}$, $N_{22,24}$ and $H_{77,78}$ in $H_2S_2PP^{2+}$ and $H_{25,78,79}$, S_{23} and $N_{21,22,24}$ in H_3SPP^{2+}. It is of importance to note, that a significant summarized charge in H_3SPP^{2+} (-1.91e) makes it impossible to coordinate the anions, such as ClO_4^- of perchloric acid. In contrast, this charge in $H_2S_2PP^{2+}$ is twice as little, i.e. –0.97e, and the ClO_4^- coordination in this case is thus possible, that clearly depicted in the UV-vis spectra, see Fig.2(a). The repulsion between the positively charged protons and sulfur atoms of the central cavity in $H_2S_2PP^{2+}$ push them away from to the cavities' plane but in opposite directions, i.e. the S atoms are on the one side and the protons on the another by 1.57 ($S_{21,23}$) and 2.61 ($H_{77,78}$) Å, respectively. For comparison, these values for **I** are less than those of **II** and amounted to 2.27 ($H_{77,79}$) 1.53 (S) and 2.36 (H_{78}) Å, and, in combination with the cavity's charge, a coordination of anions is not favorable.

TDDFT calculations and simulation of electronic absorption spectra.

Theoretical electron absorption UV-vis spectra were simulated for $H_2S_2PP^{2+}$, HS_2PP^+, S_2PP, H_3SPP^{2+}, H_2SPP^+ and HSPP species as for the gas as well for the solutions (in terms of PCM approach) with 30 excited states taken into consideration, Figure 4. and Figure 5. It is worth noting, that an attempt of the spectra simulation with 10 excitations revealed to be clearly insufficient due to essential contribution of the higher levels being populated.

Below, we briefly discuss the spectra of the dication forms since they may be able to coordinate a counterion and, due to that, may be considered as gas-sensors.

$H_2S_2PP^{2+}$. The most intense experimental band at 445 nm with a shoulder at 414 nm may be assigned to the simulated ones at 448 nm and 420, respectively. The shoulder on the theoretical spectrum is summarized from, mainly, 426, 419, 418, 407, 405 nm bands with 0.10, 0.25, 0.20, 0.32 and 0.05 contributions, respectively, Figure 4, which are related to the electron transitions from the periphery to the central cavity.

The band at *ca*. 448 nm is composed by transitions corresponding to HOMO→LUMO with HOMO-1→ LUMO+1 (448 nm) and HOMO-1→LUMO (447 nm) orbitals which located within the central cavity.

Comparing to the experiment, the simulated 420 nm shoulder's overall contribution is overestimated, due probably to the time necessary for the closest states relaxation not taken into account correctly.

H_3SPP^{2+}. Both. Experimental and simulated spectra are similar to that of **$H_2S_2PP^{2+}$**. The intense maximum at 443 nm in the simulated spectrum is formed by the transitions from HOMO-1 to LUMO, and HOMO to LUMO+1 molecular orbitals Figure 6, but, unlike the experiment, an additional band occurs at 409 nm which corresponds to the HOMO-7, HOMO-5, HOMO-3, HOMO-6, HOMO-4, HOMO-2 and HOMO, to the LUMO+1 and LUMO molecular orbitals, Figure 5.

As for the band at 409 nm, much more transitions contribute than to that at 443 nm, though of lower impact: from HOMO-7, HOMO-5, HOMO-3, HOMO-6, HOMO-4, HOMO-2, HOMO to LUMO+1 and LUMO. These transitions correspond to the electron density transfer from the periphery to the central cavity.

Concluding, these two most intense bands in the UV-vis spectra of the dication forms of the compounds under study **I** and **II** resulted from the main processes: the 'in-core' electron density redistributions and the 'periphery-to-central cavity' transfer, arguing an importance of the structure study of the macroheterocycle core.

Analyzing the spectra, one should note that the protonation of the neutral forms shifts the main bands to the long-wave region that is due to the energy gap reduction between HOMO-1, HOMO and LUMO, LUMO+1. Moreover, the new maxima appeared in the long-wave region over 600 nm support this observation, see Figure 4(c). and Figure 5(c).

The simulated spectra of the neutral S_2PP **II** and HSPP **I** are in a good agreement with the experiment - the theoretical main maxima at 424 and 414 nm are shifted by only 5 and 10 nm, respectively, from the measured ones, Figure 4(a) and Figure 5(a).

The significant hypsochromic shift of the theoretical maximum relative to the experiment in the ionized forms of HSPP **I** can be a result of trend of TDDFT method to overestimate the vertical excitation energies with respect to experiment. This tendency is typical for such kind of compounds, see for example [59–61].

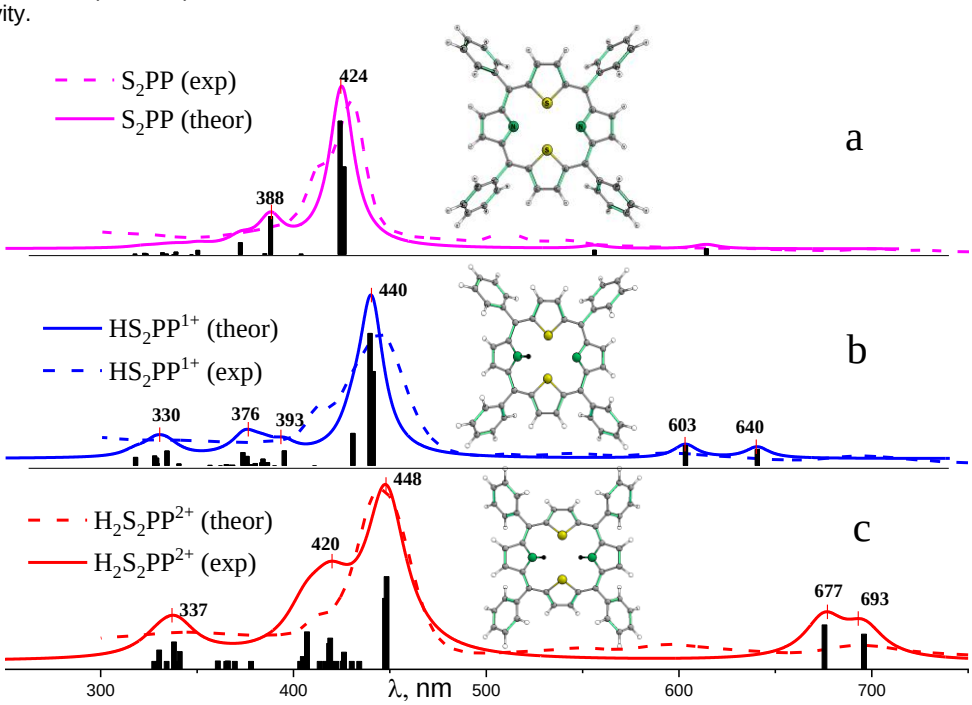

Figure 4. Experimental (dashed lines) and simulated (solid lines) UV-vis spectra of **II**: (a) neutral, cation (b) and dication (c) forms.

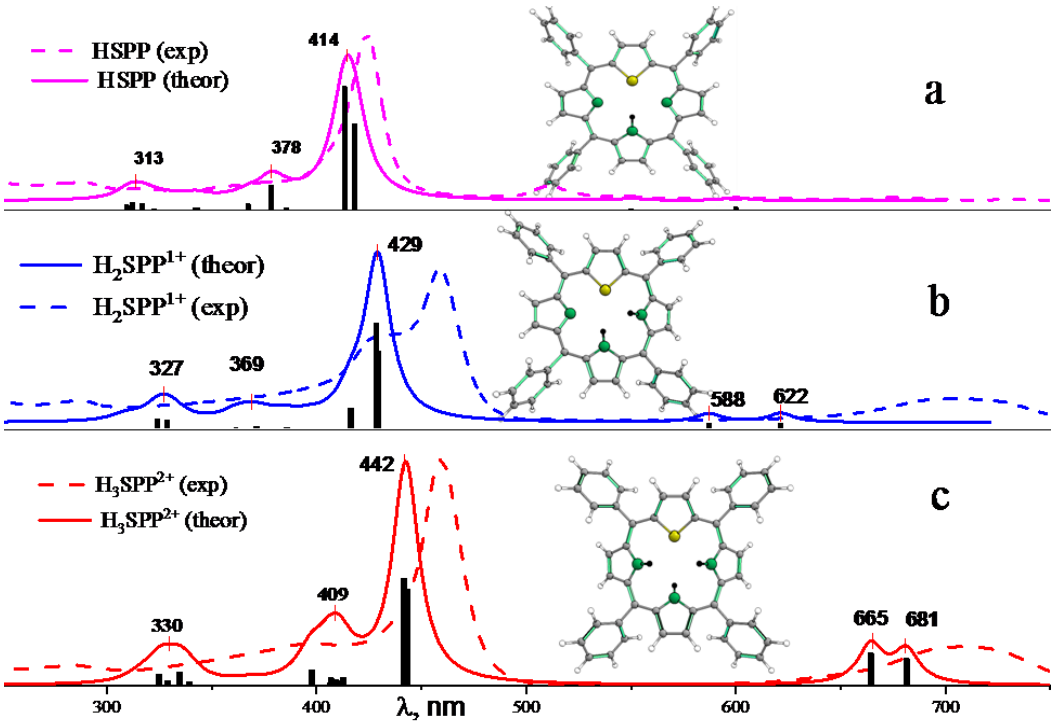

Figure 5. Experimental (dashed lines) and simulated (solid lines) UV-vis spectra of **I**: (a) neutral, cation (b) and dication (c) forms.

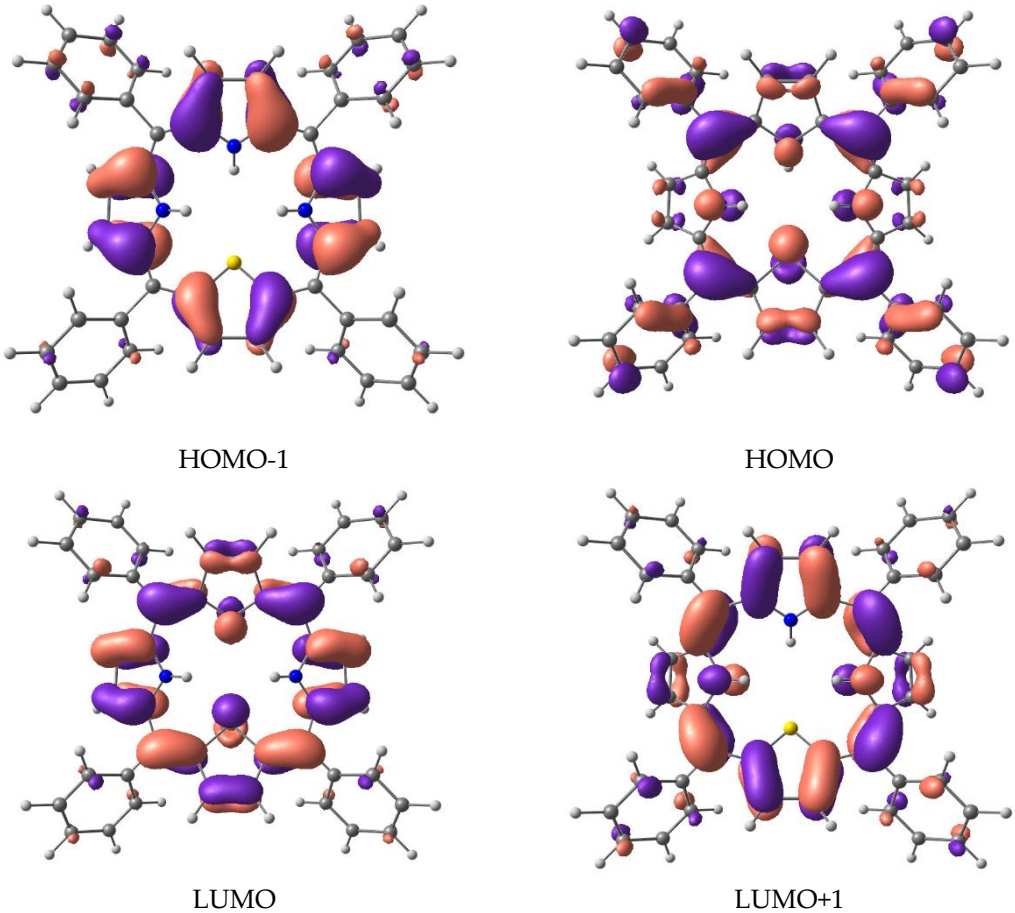

Figure 6. Molecular orbital's of H_3SPP^{+2}.

Conclusion

Protonated forms of 21.23-thio- and 21-dithio-5.10.15.20-tetraphenylporphyrins dissolved in CH_3CN were obtained at titration by $HClO_4$ at 298 K with following characterization of their properties. It was found that for the compound **I**, the ionization starts at pH=10 reaching maximum concentration of H_2SPP^+ at pH=8. For the compound **II**, the protonation starts at pH=14, and the concentration of HS_2PP^+ reaches a maximum at pH=10.5, which indicates more pronounced basic properties than of that of **I**.

It should be noted that the dicationic form of **II** is also formed under milder, as compared with **I**, conditions, and already at pH=7.5 its concentration reaches a maximum, starting at pH=10.5, while for **I** the start and the maximum correspond to pH=9 and pH=5, respectively.

Upon further titration, it was found that the doubly protonated form of **II**, $H_2S_2PP^{2+}$, is able to coordinate the ClO^{4-} counterion, unlike that of **I**. To explain this difference in the coordination ability, a quantum-chemical calculation of the equilibrium geometry of compounds **I** and **II** was performed, taking into account the interaction with the solvent, which indicated an increase in the perimeter of the cavity upon heteroatomic substitution in the series **III**→**I**→**II** with a step of about 0.8 Å, in the both, neutral and ionized, forms. Moreover, during protonation and diprotonation, a distortion of the core plane is observed with a significant out-of-plane shift of the central atoms N, S and H for the compounds **I** and **II**. As follows from the results of the QTAIM calculations, the central cavity of H_3SPP^{2+} bears twice as much negative charge as $H_2S_2PP^{2+}$, which indicates a higher ability to coordinate the counterions (ClO^{4-}) by the cavity of the latter. The UV-vis spectra simulated by TDDFT match the experimental data in reproducing the trend of the spectra changes during titration in the series neutral→cation→dication for **I** and **II**.

The results obtained in this work can serve as a theoretical basis for obtaining the active components of highly sensitive anion-selective materials based on heterosubstituted porphyrinoids.

Experimental Section

Syntheses.

A general procedure was used to synthesize meso-substituted 21-thia and 21, 23-dithia porphyrins.

1 mole of 2,5-thienediylbis(phenylmethanol), synthesized as described in [32,58,62], was condensed with 2 moles of arylaldehyde and 3 moles of pyrrole under porphyrin forming conditions [63] to obtain 21-thia-substituted porphyrin **I**, yield 15.7%. Dithiaporphyrin **II** was isolated as a by-product, yield 3.2%, see Scheme 1. This compound was purification by column chromatography on Al_2O_3 (III active stage by Brecman), eluent – dichloromethane. The control of purity of the compound was carried out by TLC method, used Silufol (Merck) plate with a thickness of active layer 0.5 mm and an eluent CH_2Cl_2. Spectral characteristic of molecules I and II satisfy the literature [34,35,62].

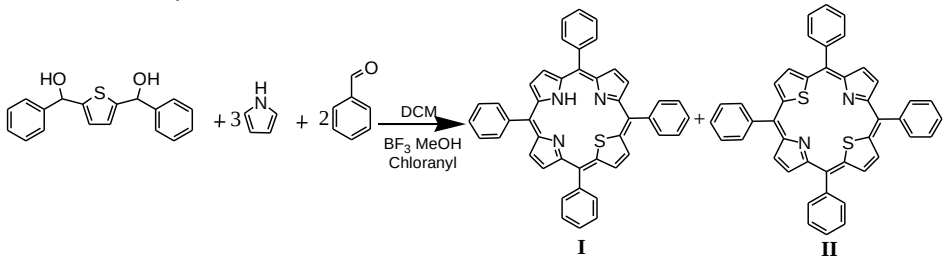

Scheme 1.

Spectroscopic experiments.

The IR - spectra were recorded by Avatar 360 FT-IR spectrophotometer ("Thermo Nicolet", USA) in KBr pellets (approximately 1 mg porphyrin / 100 mg KBr) in the frequency region 400 - 4000 cm^{-1} at room temperature. The ^1H NMR spectra were recorded by Bruker-500 spectrometer at the operating frequency 500 MHz, in $CDCl_3$, internal reference TMS. UV-Vis spectra were recorded by two-beam spectrometers "Shimadzu UV-180", using a quartz cell with optical pathways of 1 mm and 10 mm in acetonitrile (hereinafter referred as ACN) and CH_2Cl_2

Computational details.

A hybrid DFT computational method with B3LYP functional and cc-pVTZ basis set was used for all calculations. Geometry optimizations were performed for HSPP, S_2PP and their protonated ionic forms HS_2PP^+, $H_2S_2PP^{2+}$, H_2SPP^+ and H_3SPP^{2+}, followed by calculations of vibrational harmonic frequencies in order to confirm whether the optimized structures are minima on the potential energy hyper-surface. The ACN solvent environment was modeled by employing the PCM method. The solvation effects (with ACN) were introduced by the Self-Consistent Reaction Field (SCRF); this keyword requests that a calculation is performed in the presence of a solvent by placing the solute in a cavity within the solvent reaction field using the CPCM polarizable conductor calculation model. The UV–Vis absorption spectra for the ionic and neutral forms of the studied dyes in ACN were simulated using TD-DFT method. All calculations have been realized for the closed-shell electronic state. The Gaussian09 software [64] was used for calculations.

The topological analysis of electron density distribution function $\rho(r)$ in terms of quantum theory atoms in molecule (QTAIM) was carried out using AIMAll Professional software [65]. The visualizations of molecular models were realized by Chemcraft [66] program.

The geometrical parameters (as sets of Cartesian coordinates) of the complexes are listed in ESI.

Funding: This work is supported by the Russian Science Foundation (grant № 21-73-10126).

Acknowledgements

The research was carried out using the resources of the Center for Shared Use of Scientific Equipment of the ISUCT (with the support of the Ministry of Science and Higher Education of Russia, grant No. 075-15-2021-671).

Keywords: thiaporphyrins; coordination properties; acid-base properties; quantum chemical calculations; UV–Vis absorption spectra.

Reference

[1] M. J. F. Calvete, S. M. A. Pinto, M. M. Pereira, C. F. G. C. Geraldes, *Coord. Chem. Rev.* **2017**, *333*, 82–107.
[2] F. Giuntini, R. Boyle, M. Sibrian-Vazquez, M. Graça H. Vicente, **2013**, pp. 303–416.
[3] N. Sekkat, H. van den Bergh, T. Nyokong, N. Lange, *Molecules* **2011**, *17*, 98–144.
[4] M. Calvete, A. Simoes, C. Henriques, S. Pinto, M. Pereira, *Curr. Org. Synth.* **2014**, *11*, 127–140.
[5] A. V. C. Simões, A. Adamowicz, J. M. Dąbrowski, M. J. F. Calvete, A. R. Abreu, G. Stochel, L. G. Arnaut, M. M. Pereira, *Tetrahedron* **2012**, *68*, 8767–8772.
[6] S. M. A. Pinto, V. A. Tomé, M. J. F. Calvete, M. M. Pereira, H. D. Burrows, A. M. S. Cardoso, A. Pallier, M. M. C.A. Castro, É. Tóth, C. F. G. C. Geraldes, *J. Inorg. Biochem.* **2016**, *154*, 50–59.
[7] A. V. C. Simões, S. M. A. Pinto, M. J. F. Calvete, C. M. F. Gomes, N. C. Ferreira, M. Castelo-Branco, J. Llop, M. M. Pereira, A. J. Abrunhosa, *RSC Adv.* **2015**, *5*, 99540–99546.
[8] D. Mansuy, *Comptes Rendus Chim.* **2007**, *10*, 392–413.
[9] Y. S. Marfin, • A S Vashurin, • E V Rumyantsev, • S G Puhovskaya, **n.d.**, DOI 10.1007/s10971-013-3009-6.
[10] M. J. F. Calvete, M. Silva, M. M. Pereira, H. D. Burrows, *RSC Adv.* **2013**, *3*, 22774.
[11] L. Cuesta-Aluja, J. Castilla, A. M. Masdeu-Bultó, C. A. Henriques, M. J. F. Calvete, M. M. Pereira, *J. Mol. Catal. A Chem.* **2016**, *423*, 489–494.
[12] T. Tanaka, A. Osuka, *Chem. Soc. Rev.* **2015**, *44*, 943–969.
[13] L. L. Li, E. W. G. Diau, *Chem. Soc. Rev.* **2013**, *42*, 291–304.
[14] D. Dini, M. J. F. Calvete, M. Hanack, *Chem. Rev.* **2016**, *116*, 13043–13233.
[15] M. J. F. Calvete, *Int. Rev. Phys. Chem.* **2012**, *31*, 319–366.
[16] S. M. A. Pinto, Â. C. B. Neves, M. J. F. Calvete, A. R. Abreu, M. T. S. Rosado, T. Costa, H. D. Burrows, M. M. Pereira, *J. Photochem. Photobiol. A Chem.* **2012**, *242*, 59–66.
[17] A. T. Marques, S. M. A. Pinto, C. J. P. Monteiro, J. S. Seixas De Melo, H. D. Burrows, U. Scherf, M. J. F. Calvete, M. M. Pereira, *J. Polym. Sci. Part A Polym. Chem.* **2012**, *50*, 1408–1417.
[18] K. M. Kadish, K. M. Smith, R. Guilard, *In Porphyrin Handbook*, Singapore, **2000**.
[19] T. Kaur, W. Z. Lee, M. Ravikanth, *Inorg. Chem.* **2016**, *55*, 5305–5311.
[20] M. J. Białek, L. Latos-Grazyński, *Inorg. Chem.* **2016**, *55*, 1758–1769.
[21] P. Chmielewski, M. Grzeszczuk, L. Latos-Grazynski, J. Lisowski, *Inorg. Chem.* **1989**, *28*, 3546–3552.
[22] L. Latos-Grazynski, J. Lisowski, M. M. Olmstead, A. L. Balch, *Inorg. Chem.* **1989**, *28*, 3328–3331.
[23] L. Latos-grazynski, M. M. Olmstead, A. L. Balch, *Inorg. Chem.* **1989**, *28*, 4065–4066.
[24] J. Lisowski, M. Grzeszczuk, L. Latos-Grażynski, *Inorganica Chim. Acta* **1989**, *161*, 153–163.
[25] R. P. Pandian, T. K. Chandrashekar, *Inorg. Chem.* **1994**, *33*, 3317–3324.
[26] C. S. Gopinath, R. P. Pandian, P. T. Manoharan, *J. Chem. Soc. - Dalt. Trans.* **1996**, 1255–1259.
[27] P. J. Chmielewski, L. Latos-Grażyński, M. M. Olmstead, A. L. Balch, *Chem. - A Eur. J.* **1997**, *3*, 268–278.
[28] P. J. Chmielewski, L. Latos-Grażyński, *Inorg. Chem.* **1998**, *37*, 4179–4183.
[29] B. Sridevi, S. J. Narayanan, A. Srinivasan, T. K. Chandrashekar, J. Subramanian, *J. Chem. Soc. Dalt. Trans.* **1998**, *9*, 1979–1984.
[30] L. Latos-Grażyński, J. Lisowski, P. Chmielewski, M. Grzeszczuk, M. M. Olmstead, A. L. Balch, *Inorg. Chem.* **1994**, *33*, 192–197.
[31] L. Latos-Grażyński, E. Pacholska, P. J. Chmielewski, M. M. Olmstead, A. L. Balch, *Inorg. Chem.* **1996**, *35*, 566–573.
[32] Z. Gross, I. Saltsman, R. P. Pandian, C. M. Barzilay, *Tetrahedron Lett.* **1997**, *38*, 2383–2386.
[33] L. LATOS-GRAZYNSKI, P. J. CHMIELEWSKI, *ChemInform* **2010**, *28*, no-no.
[34] P. J. Chmielewski, L. Latos-Grażyński, *Inorg. Chem.* **1992**, *31*, 5231–5235.
[35] E. Pacholska, P. J. Chmielewski, L. Latos-Grażyński, *Inorganica Chim. Acta* **1998**, *273*, 184–190.
[36] I. V. Vershilovskaya, L. S. Liulkovich, S. G. Pukhovskaya, Y. B. Ivanova, A. O. Plotnikova, M. M. Kruk, *J. Appl. Spectrosc.* **2020**, *87*, 201–207.
[37] J. M. Pedrosa, C. M. Dooling, T. H. Richardson, R. K. Hyde, C. A. Hunter, M. T. Martín, L. Camacho, *J. Mater. Chem.* **2002**, *12*, 2659–2664.
[38] M. Zawadzka, J. Wang, W. J. Blau, M. O. Senge, *J. Porphyr. Phthalocyanines* **2013**, *17*, 1129–1133.
[39] Hambright P., S. K.M., *Porphyrins and Metalloporphyrins.*, Elsevier Scientific Publishing Company, Amsterdam, **1975**.
[40] S. Thyagarajan, T. Leiding, S. P. Årsköld, A. V. Cheprakov, S. A. Vinogradov, *Inorg. Chem.* **2010**, *49*, 9909–9920.
[41] A. B. Rudine, B. D. Delfatti, C. C. Wamser, *J. Org. Chem.* **2013**, *78*, 6040–6049.
[42] R. J. Abraham, G. E. Hawkes, K. M. Smith, *Tetrahedron Lett.* **1974**, *15*, 71–74.
[43] S. G. Pukhovskaya, Y. B. Ivanova, D. T. Nam, A. S. Vashurin, *Russ. J. Phys. Chem. A* **2014**, *88*, 1670–1676.
[44] I. Gupta, M. Ravikanth, *J. Photochem. Photobiol. A Chem.* **2006**, *177*, 156–163.
[45] R. P. Pandian, D. Reddy, N. Chidambaram, T. K. Chandrashekar, *Proc. / Indian Acad. Sci.* **1990**, *102*, 307–318.
[46] I. V Vershilovskaya, L. S. Liulkovich, S. G. Pukhovskaya, Y. B. Ivanova, A. O. Plotnikova, M. M. Kruk, *J. Appl. Spectrosc.* **2020**, *87*, 201–207.
[47] V. G. Andrianov, O. V. Malkova, *Macroheterocycles* **2009**, *2*, 130–138.
[48] M. M. Kruk, A. S. Starukhin, W. Maes, *Macroheterocycles* **2011**, *4*, 69–79.
[49] K. Tagawa, S. Mori, T. Okujima, M. Takase, H. Uno, *Tetrahedron* **2017**, *73*, 794–801.
[50] A. N. Gurinovich, K. N. Sevchenko, *Solovyov Spectroscopy of Chlorophyll and Related Compounds*, Science And Technology, Minsk, **1968**.
[51] I. M. Kolthoff, M. K. Chantooni, S. Bhowmik, *Anal. Chem.* **1967**, *39*, 1627–1633.
[52] Y. B. Ivanova, V. B. Sheinin, N. Z. Mamardashvili, *Russ. J. Gen. Chem.* **2007**, *77*, 1458–1462.
[53] M. M. Kruk, Y. B. Ivanova, V. B. Sheinin, A. S. Starukhin, N. Z. Mamardashvili, O. I. Koifman, *Macroheterocycles* **2008**, *1*, 50–58.
[54] J. R. Reimers, L. E. Hall, *J. Am. Chem. Soc.* **1999**, *121*, 3730–3744.
[55] L. Pauling, *The Nature of the Chemical Bond and the Structure of Molecules and Crystals: An Introduction to Modern Structural Chemistry*, **1960**.
[56] I. Y. Kurochkin, A. E. Pogonin, A. A. Otlyotov, A. N. Kiselev, A. V. Krasnov, S. A. Shlykov, G. V. Girichev, *J. Mol. Struct.* **2020**, *1221*, DOI 10.1016/j.molstruc.2020.128662.
[57] T. Chatterjee, V. S. Shetti, R. Sharma, M. Ravikanth, *Chem. Rev.* **2017**, *117*, 3254–3328.
[58] C. H. Lee, W. S. Cho, *Tetrahedron Lett.* **1999**, *40*, 8879–8882.
[59] P. A. Stuzhin, S. S. Ivanova, M. Hamdoush, G. A. Kirakosyan, A. Kiselev, A. Popov, V. Sliznev, C. Ercolani, *Dalt. Trans.* **2019**, DOI 10.1039/c9dt02345c.
[60] J. Mack, Y. Asano, N. Kobayashi, M. Stillman, *J. Am. Chem. Soc.* **2005**, DOI 10.1021/ja0540728.
[61] J. Mack, J. Stone, T. Nyokong, *J. Porphyr. Phthalocyanines* **2014**, DOI 10.1142/S108842461450045X.
[62] L. Latos-grazynski, J. Lisowski, M. M. Olmstead, A. L. Balch, *J. Am. Chem. Soc.* **1987**, *109*, 4428–4429.
[63] A. Ulman, J. Manassen, *J. Am. Chem. Soc.* **1975**, *97*, 6540–6544.

[64] M. J. Frisch, G. W. Trucks, H. B. Schlegel, G. E. Scuseria, M. A. Robb, J. R. Cheeseman, G. Scalmani, V. Barone, G. A. Petersson, H. Nakatsuji, X. Li, M. Caricato, A. Marenich, J. Bloino, B. G. Janesko, R. Gomperts, B. Mennucci, H. P. Hratchian, J. V. Ortiz, A. F. Izmaylov, J. L. Sonnenberg, D. Williams-Young, F. Ding, F. Lipparini, F. Egidi, J. Goings, B. Peng, A. Petrone, T. Henderson, D. Ranasinghe, V. G. Zakrzewski, J. Gao, N. Rega, G. Zheng, W. Liang, M. Hada, M. Ehara, K. Toyota, R. Fukuda, J. Hasegawa, M. Ishida, T. Nakajima, Y. Honda, O. Kitao, H. Nakai, T. Vreven, K. Throssell, J. A. Montgomery Jr., J. E. Peralta, F. Ogliaro, M. Bearpark, J. J. Heyd, E. Brothers, K. N. Kudin, V. N. Staroverov, T. Keith, R. Kobayashi, J. Normand, K. Raghavachari, A. Rendell, J. C. Burant, S. S. Iyengar, J. Tomasi, M. Cossi, J. M. Millam, M. Klene, C. Adamo, R. Cammi, J. W. Ochterski, R. L. Martin, K. Morokuma, O. Farkas, J. B. Foresman, D. J. Fox, *Gaussian Inc., Wallingford, CT* **2016**.

[65] T. A. Keith, T. Gristmill, AIMAII**.**

[66] Zhurko, G.A.; Zhurko, D.A. ChemCraft Version 1.6 (Build 312); Version 1.6 (Build 312) Ed. Available online: **http://www.chemcraftprog.com/index.html** (accessed on 28 December 2020).